Laser and Particle Beams (2003), *21*, 455–461. Printed in the USA.

DOI: 10.1017/S0263034603213264

Arbitrary Lagrange–Eulerian code simulations of turbulent Rayleigh–Taylor instability in two and three dimensions

S.V. WEBER,[1] G. DIMONTE,[2] AND M.M. MARINAK[1]

[1]Lawrence Livermore National Laboratory, Berkeley, California
[2]Los Alamos National Laboratory, Los Alamos, New Mexico

(RECEIVED 8 July 2002; ACCEPTED 4 April 2003)

Abstract

We have performed simulations of the evolution of the turbulent Rayleigh–Taylor instability with an arbitrary Lagrange–Eulerian code. The problem specification was defined by Dimonte *et al.* (2003) for the "alpha group" code intercomparison project. Perfect $\gamma = 5/3$ gases of densities 1 and 3 g/cm^3 are accelerated by constant gravity. The nominal problem uses a $256^2 \times 512$ mesh with initial random multiwavelength interface perturbations. We have also run three-dimensional problems with smaller meshes and two-dimensional (2D) problems of several mesh sizes. Underresolution lowered linear growth rates of the seed modes to 5-60% of the analytic values, depending on wavelength and orientation to the mesh. However, the mix extent in the 2D simulations changed little with grid refinement. Simulations without interface reconstruction gave penetration only slightly reduced from the case with interface reconstruction. Energy dissipation differs little between the two cases. The slope of the penetration distance versus time squared, corresponding to the α parameter in $h = \alpha A g t^2$, decreases with increasing time in these simulations. The slope, α, is consistent with the linear electric motor data of Dimonte and Schneider (2000), but the growth is delayed in time.

Keywords: Arbitrary Lagrange–Eulerian code; Rayleigh–Taylor instability; Turbulent

1. INTRODUCTION

Turbulent mixing driven by the Rayleigh–Taylor (RT) instability is an important physical process in a number of environments, including inertial confinement fusion (Lindl, 1995). Perturbations at an accelerated material interface grow by the RT instability when the direction of acceleration is from the lighter material toward the heavier material. If perturbations are small in amplitude compared to wavelength, then the growth is described by linear theory, giving the amplitude of a perturbation of wavenumber, k, varying with time, t, as $a_k \propto e^{\gamma t}$, where the growth rate $\gamma = (Agk)^{1/2}$. Here, g is the acceleration, $A = (\rho_h - \rho_l)/(\rho_h - \rho_l)$ is the Atwood number, and ρ_h and ρ_l are the densities of the heavy and light fluids (Rayleigh, 1900; Taylor, 1950). When $ka_k \sim 1$, nonlinear effects become important. These include coupling of different wavelengths, changes in shape of the modulation, and reduction in the rate of growth below exponential. A surface with multiwavelength initial perturbations eventually will develop into a mixing zone of turbulent, multiscale structure. Experiments (Read, 1984), simulations, and scaling arguments (Annuchina *et al.*, 1978; Youngs, 1984) indicate that the mixing region should grow with time in a self-similar fashion, and that the total mixing extent should increase as $h = \alpha A g t^2$.

Two-dimensional (2D) and three-dimensional (3D) simulations of this process have been presented by a number of authors (including Youngs, 1994; Hecht *et al.*, 1995; Cook and Dimotakis, 2001; Glimm *et al.*, 2001; Young *et al.*, 2001). Fits to the parameter, α, vary, but the simulated problems and analysis methods also differ. For this reason, a test problem was proposed (Dimonte *et al.*, 2003) to permit comparisons between codes for identical conditions. This article reports only upon our own work; results of other groups, comparisons, and general conclusions are presented elsewhere (Dimonte *et al.*, 2003). The problem specifies constant acceleration, compressible γ-law gases, and defines the mesh and the initial interface perturbation.

We present simulations of the "α group" test problem (Dimonte *et al.*, 2003) employing an arbitrary Lagrange–Eulerian (ALE) code, HYDRA (Marinak *et al.*, 1996). HYDRA incorporates interface reconstruction, but the full problem has only been run without this. We have also run

Address correspondence and reprint requests to: Stephen Weber, Lawrence Livermore National Laboratory, P.O. Box 808, Livermore, CA 94551. E-mail: weber8@llnl.gov

smaller simulations, either $128^2 \times 256$ or $128^2 \times 512$, and either with and without interface reconstruction. We find that interface reconstruction gives only slightly larger penetration distances, and little difference in the energy dissipation rate.

We have performed 2D simulations with meshes of 256×512, 512×1024, and 1024×2048, using a cut of the 3D initial perturbation. The initial modulation was held constant while the mesh size increased, so that the larger problems better resolve the initial structure. Although the nominal problem greatly undercalculated the linear growth rates of the initial perturbations, the mix extent at late times differed little between these resolutions.

2. PROBLEM DEFINITION

The test problem specifies perfect gases of $\gamma = 5/3$ in a box of width and depth, $L = 10$ cm, and height $2L$. The light and heavy layers have heights $17L/16$ and $15L/16$. Gravity is taken to be in the z direction. The initial density distribution is

$$\rho = \rho_0 \left(1 - \frac{\gamma - 1}{\gamma} \frac{\rho_0 g z}{P_0}\right)^{1/(\gamma-1)}$$

where $P_0 = 500$ dyne/cm^2, $\rho_0 = 3$ g/cm^3 for the top fluid, $\rho_0 = 1$ g/cm^3 for the lower fluid, and $g = 2$ cm/s^2. The mesh is $256^2 \times 512$. The initial perturbations have a random spectrum in an annulus in k space spanning 32–64 wavelengths across the box width. The modal amplitudes are selected from a Gaussian of rms 0.1 cm. The surface was intended to be the same for all simulations. The upper and lower boundaries are rigid walls.

The original surface was created for use with periodic spanwise boundaries. Thus, it was constructed of modes having random phases with respect to the boundaries. The ALE code that we have used, HYDRA, did not provide periodic boundary conditions (bc) at the time we began this study, but they were added later. The modes supported on a square domain with reflection boundaries are $\cos(\pi nx/L)$ $\cos(\pi my/L)$. If the original surface is evolved with reflection boundary conditions, the modes with sine components are aliased into cosine modes, creating higher spatial frequencies. Equivalently, treating the sine modes as reflection symmetric results in a cusp at the boundary. This yields apparently spurious growth at the boundaries, even in the linear regime.

Consequently, Youngs (2001, pers. comm.) provided an alternative surface of otherwise equivalent statistics made up of normal modes for reflection boundaries. The number of modes in the **k** space annulus is equal to that for the periodic case because modes may have a half-integer number of wavelengths across the domain. The two initial surfaces and resulting early evolution appear very similar.

HYDRA (Marinak *et al.*, 1996) is an ALE code with interface reconstruction. Because the two materials have the same γ, we can treat them either as the same fluid starting at different adiabats or as two fluids. In the second case, interface reconstruction is performed, whereas in the first case, it is not. Without interface reconstruction, advection of the interface results in mixing of the two materials.

3. RESOLUTION ISSUES

The resolution of the initial perturbations of 4–8 zones per wavelength significantly affects the accuracy of the results. Underresolution acts like a viscosity, slowing the growth of shorter wavelengths. This choice of modes resulted from a trade-off between resolution and dynamic range in wave number. Youngs (1994) found that this resolution appeared to give convergence in the growth of mix width.

Figure 1 shows the ratio of the growth rate in the linear regime to the analytic value $(gkA)^{1/2}$. In the 2D runs, the initial perturbations grow at 15–40% of the analytic rate. In 3D, modes with **k** oblique to the mesh grow even more slowly, down to 5% of the analytic rate. As a consequence of this orientation dependence, the perturbation evolves from random in the x–y plane to a checkerboard pattern of prominent bubbles during linear growth. Mesh alignment is not apparent in later stages in the flow.

Youngs (2001, pers. comm.) noted that terminal bubble velocities, which may be more relevant to self-similar growth, converged more rapidly with zoning than linear growth rates. Figure 2 shows bubble rise velocities for simulations of a 3D single bubble in a square box. Convergence in terminal

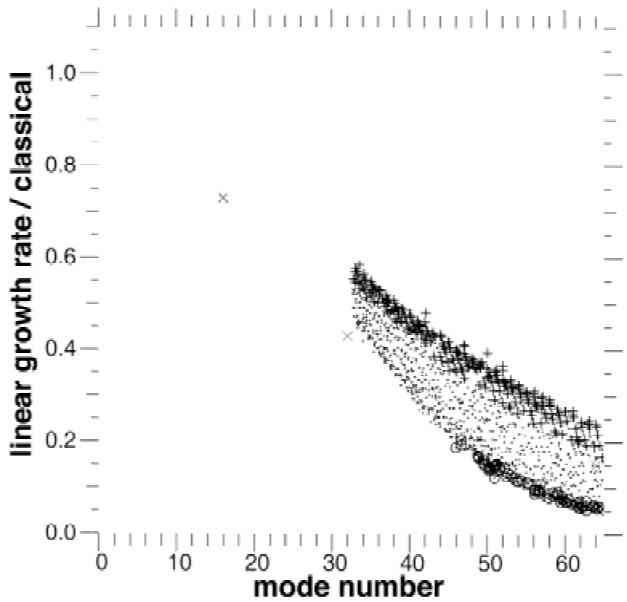

Fig. 1. Ratio of linear growth rate to classical incompressible value versus mode number, that is, number of wavelengths in $L = 10$ cm. xs are results from 2D single-mode simulations, and other symbols are from the near-linear regime of 3D multimode simulations; +: modes with **k** nearly parallel to the boundaries, ○: **k** near diagonal to boundaries, ·: intermediate angles.

https://doi.org/10.1017/S0263034603213264 Published online by Cambridge University Press

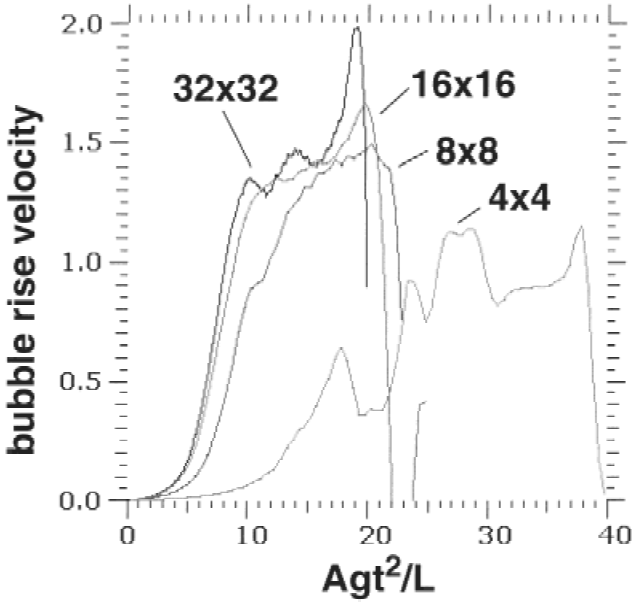

Fig. 2. Bubble rise velocity (cm/s) versus Agt^2/L for single 3D bubbles in a 10×10 cm box, for different mesh resolutions.

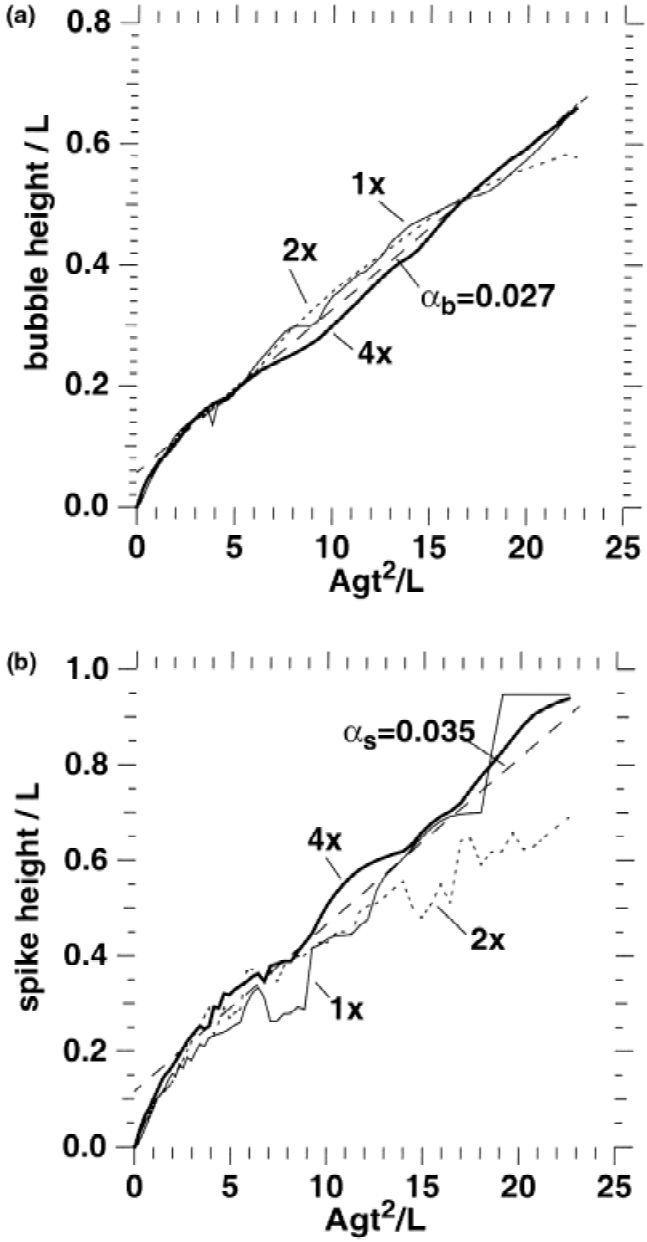

Fig. 3. a: Bubble height/L, $L = 10$ cm versus Agt^2/L, from 2D simulations of different meshes, 1x: 256×512 (thin solid), 2x: 512×1024 (dotted), 4x: 1024×2048 (thick solid); b: similar, but for spikes. Dashed curves are lines of constant α, slope $\alpha_b = 0.027$ for bubbles, $\alpha_s = 0.035$ for spikes.

bubble velocity is seen by 8 zones per wavelength, but the time needed to reach terminal velocity depends on resolution.

We have carried out a zoning refinement study in 2D simulations, with meshes of 256×512, 512×1024, and 1024×2048. The initial perturbation was the same cut of the 3D case for all three runs. Rigid boundaries were employed, resulting in artifacts that will be discussed later.

Figure 3 shows bubble and spike penetration versus time, taken as 1% and 99% volume fraction of the light material, respectively. No trend with zoning refinement is apparent. Noise is present in any particular simulation because there are a finite number of bubbles and spikes in any particular statistical realization. The number of features becomes smaller with time because of the inverse cascade. This has been noted and examined by Clark and Harlow (2002). The noise is larger in two dimensions than in three dimensions because the number of features of given size is smaller.

4. THREE-DIMENSIONAL SIMULATIONS

Three-dimensional simulations were carried out both for the nominal $256^2 \times 512$ problem (case A) and for smaller problems of either $128^2 \times 512$ (case B) or $128^2 \times 256$ (case C). Cases B and C have been run both with and without interface reconstruction, whereas the full-scale problem has been run only without interface reconstruction because of computational cost. Case B used one quadrant of the initial perturbations of the full problem, in a 5×5 cm spanwise domain, whereas case C also used a quadrant of case A perturbations, but in a 10×10 cm box and with doubled initial amplitudes and wavelengths. Case A has been simulated both with reflection and with periodic spanwise bc, whereas case B has been run only with reflection bc, and case C only with periodic bc.

Our initial simulations were performed with reflection spanwise boundary conditions (rigid walls). We observed that the most penetrating features at late times were always found on the boundaries, especially on the corners. It seems likely that the higher symmetry of the flow forced by the bc caused greater mix penetration near the boundaries. Later simulations employed periodic spanwise boundary conditions. We found that the mix penetration away from the reflection boundaries agreed well with the penetration cal-

https://doi.org/10.1017/S0263034603213264 Published online by Cambridge University Press

culated with periodic boundaries. The penetration for the full span using reflection boundaries exceeded that with periodic boundaries by as much as 30%.

Simulations with and without interface reconstruction differ little in penetration distance, although density structure in the two cases differs vastly. Figure 4 compares densities on cuts parallel to the x–z plane for case C, with and without interface reconstruction. The total mixing extent is very similar for the two cases. However, with interface reconstruction, large-scale features are broken into small droplets in which the two original fluids remain distinct, whereas without interface reconstruction, large structures are composed of mixed fluid of intermediate density. The penetration with interface reconstruction is consistently greater by ~5% than that without it. Spanwise-averaged volume fraction profiles are also close for both cases.

Figure 5 shows bubble and spike height versus Agt^2/L, for 3D simulations without interface reconstruction and for all three meshes. Cases A and B have the same initial perturbations, so they evolve very similarly until the growth is

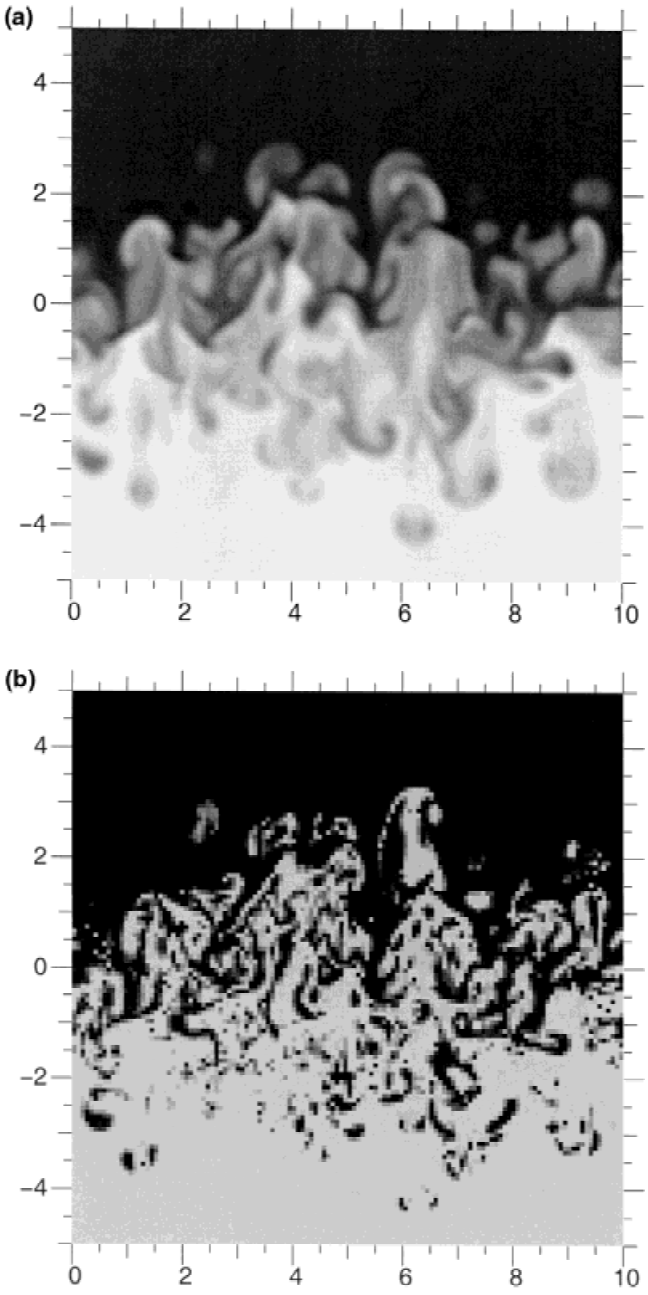

Fig. 4. Density (x, z) from case C simulations with periodic bc, on the plane $y = 2.85$ cm at a time of 8 s. a: simulation without interface reconstruction, b: simulation with interface reconstruction.

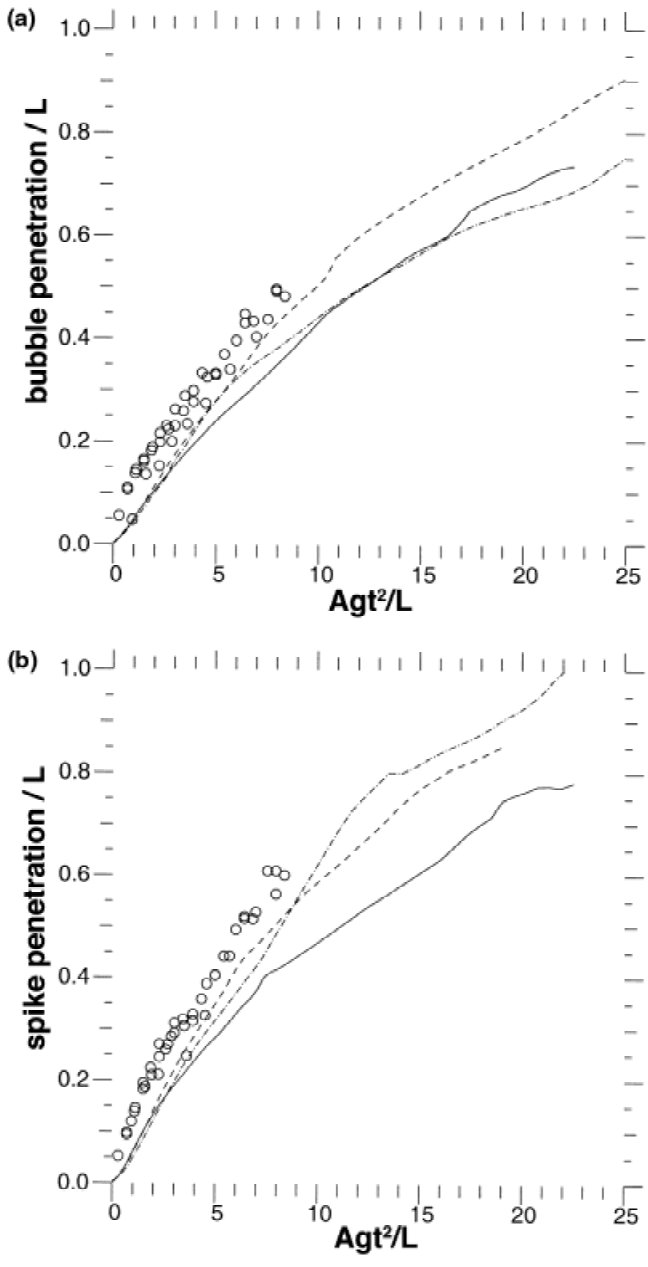

Fig. 5. a: Bubble amplitude/L versus Agt^2/L for case A ($L = 10$ cm, solid), case B ($L = 5$ cm, dot-dashed), and case C ($L = 10$ cm, dashed) simulations without interface reconstruction. Circles are LEM data of Dimonte and Schneider (2000). b: Spike amplitudes/L, similarly.

https://doi.org/10.1017/S0263034603213264 Published online by Cambridge University Press

affected by the boundaries. The bubble histories for cases A and B nearly overlay, but the spike growth appears to be less affected by the boundaries, so scaling by L does not cause the spike growth histories to collapse. The bubble and spike penetrations for case C grow initially at the same rates as in the other two cases, but show a slower decrease in growth rate with increasing time, resulting in greater penetration at later times. The difference between this simulation and the other two must result from the longer wavelengths of the initial interface perturbation.

Bubble and spike penetrations without interface reconstruction and at volume fractions of 5% and 95% are smaller than those at volume fractions 1% and 99% by a factor of ~0.75. There is less reduction for the case with interface reconstruction, by factors of 0.88 for the bubbles and 0.8 for the spikes. Most of the literature presents mix extents to the extremes of the mix region, more nearly represented by the 1% to 99% limits.

Figure 6 shows the instantaneous α, that is, the slope of $h(Agt^2)$, versus time. All cases show a monotonic (other than what appears to be statistical noise) decrease of α versus time. If the self-similarity hypothesis is correct, the slope should approach an asymptotic constant, which would be the true α of the self-similar regime. It is not convincing that the simulations exhibit an approach to self-similarity. Allowing for the possibility of a time offset, that is, $h = \alpha Ag(t - t_0)^2$, does not change the conclusion. The limited range in wavelengths, constrained on one end by grid resolution and on the other by the domain size, may prevent the achievement of a self-similar growth range. It may be tempting to take the late-time slope as the asymptotic limit. However, the boundaries constrain the growth of bubbles and may depress the late-time growth rate. We believe that the slower drop in $\alpha(Agt^2)$ of case C is a consequence of the presence of longer wavelengths in the initial surface.

Bubble and spike penetrations from the Dimonte and Schneider (2000) linear electric motor (LEM) experiment, constant acceleration $A = 0.5$ case, are also shown in Figure 5. Note that the scaling between the simulations and the experiment was based upon the domain width, L. The other length scales in this problem are the initial amplitude and wavelength, which are unknown for the LEM experiment. The fact that data show a nearly constant slope is consistent with the hypothesis that the initial perturbations do not matter. However, the simulations do not show a constant slope, so the choice of scaling affects the fit to the data, and the domain width may not be the best choice. The data agree most closely with case C, and give a larger α than the late-time slope of any of the simulations. The discrepancies could result from weaknesses in the simulations or could indicate the presence of longer-wavelength perturbations in the (poorly known) initial surface finish of the experiment.

Comparison of our results for 3D multimode RT instability to others in the literature is complicated by the fact that different studies employ different conditions. This fact was the principal reason for the alpha-group collaboration. Dimonte *et al.* (2003) present a comparison of results for identical parameters from several research groups including David Youngs and the University of Chicago team (Young *et al.*, 2001). Growth histories agree to within roughly ±10% and α values fall within the range $\alpha_b \sim 0.025 \pm 0.003$, although the other simulations show less evidence of time variation of α than ours. Cook and Dimotakis (2001) employ the Navier–Stokes equation and three initial perturbation spectra, all different from the case considered here. Their shortest wavelength case, that is most similar to ours, shows an α coefficient that varies in time, but with a different history than our results, and with a similar time average

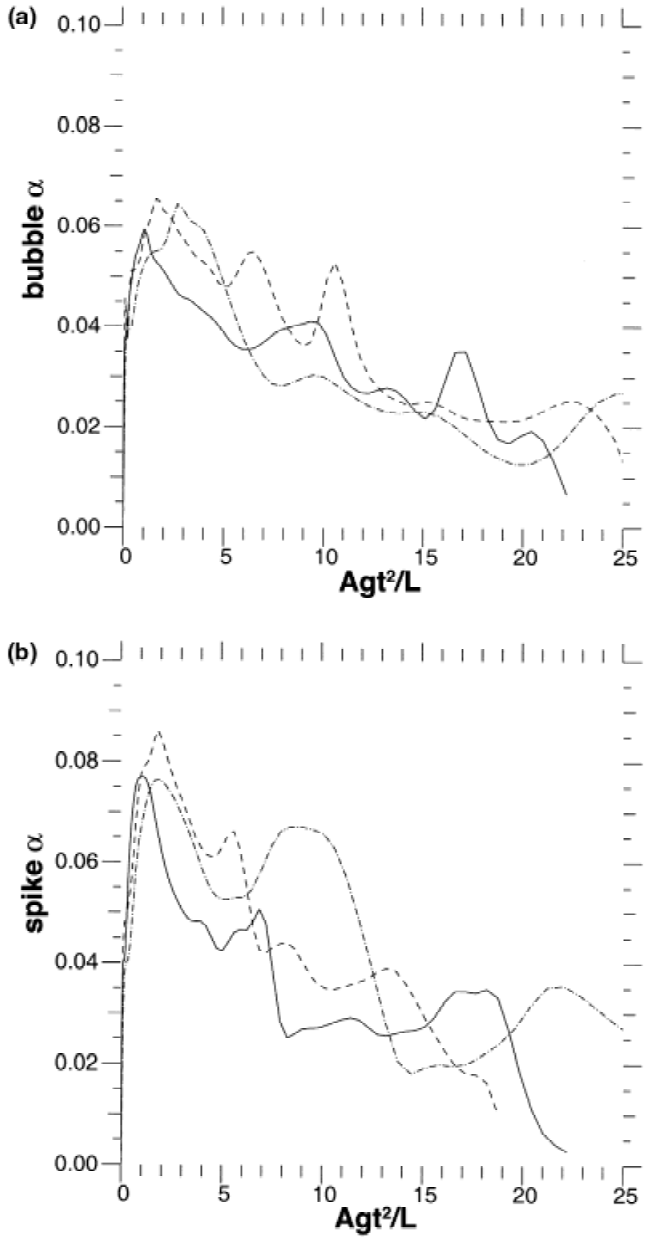

Fig. 6. a: Bubble alpha versus Agt^2/L for case A ($L = 10$ cm, solid), case B ($L = 5$ cm, dot-dashed), and case C ($L = 10$ cm, dashed) simulations without interface reconstruction. b: Spike alpha, similarly.

https://doi.org/10.1017/S0263034603213264 Published online by Cambridge University Press

$\alpha_b \sim 0.03$. Glimm *et al.* (2001) report a substantially larger value of $\alpha_b \sim 0.07$ from a front tracking code. Their initial perturbations are a longer wavelength than those of this study, 10–15 wavelengths across the box width, and also larger in initial $a/\lambda = 0.1$. This difference in α_b is consistent in sense with Cook and Dimotakis (2001), who find an increase in α_b with the mean wavelength of the initial perturbations.

An interesting parameter is the molecular mixing fraction, $\theta = \int \overline{f_1 f_2}\, dz / \int \bar{f}_1 \bar{f}_2\, dz$, where f_i is the volume fraction of fluid i, and the overbars denote averages over the spanwise plane. Figure 7 shows θ versus Agt^2/L for cases A and C. The value of θ shown for case C is an upper limit, as it is does not account for reconstructed interfaces within zones. Without interface reconstruction, $\theta \sim 0.7$, similar to results of Youngs (1994), whereas it is much smaller with interface reconstruction. Figure 7 also shows the fraction of the potential energy drop that has been dissipated and the ratio of the spanwise to streamwise kinetic energy, both for case A. These ratios are quite similar for all of the simulations, with or without interface reconstruction.

5. CONCLUSIONS

We present results of 2D and 3D simulations of growth of the Rayleigh–Taylor instability for random multimode initial roughness. The simulations employ meshes up to $256^2 \times 512$. Linear regime growth rates of the seed modes are well below the analytic values and are dependent on orientation to the mesh. However, a 2D convergence study extending to four times the nominal resolution shows no clear trend in mix extent with improved resolution.

Penetration distance and volume fraction profiles are nearly the same for simulations with and without interface reconstruction, but the small-scale structure of the mixing region is quite different. In the former case, the mixing region consists of small domains of one fluid or the other, whereas in the latter, most of the fluid in the mixing region has intermediate density.

Growth of the mix region does not appear to achieve self-similar $h = \alpha Agt^2$ form in these simulations. The instantaneous α [slope of $h(Agt^2)$] decreases with increasing time. Results for the nominal $256^2 \times 512$ problem and simulations with smaller meshes and differing initial surfaces do not overlay. One of the smaller problems gives the best agreement with the LEM data of Dimonte and Schneider (2000). It is unclear whether the experiment may have been sensitive to the initial conditions or whether these calculations do not reach the self-similar regime.

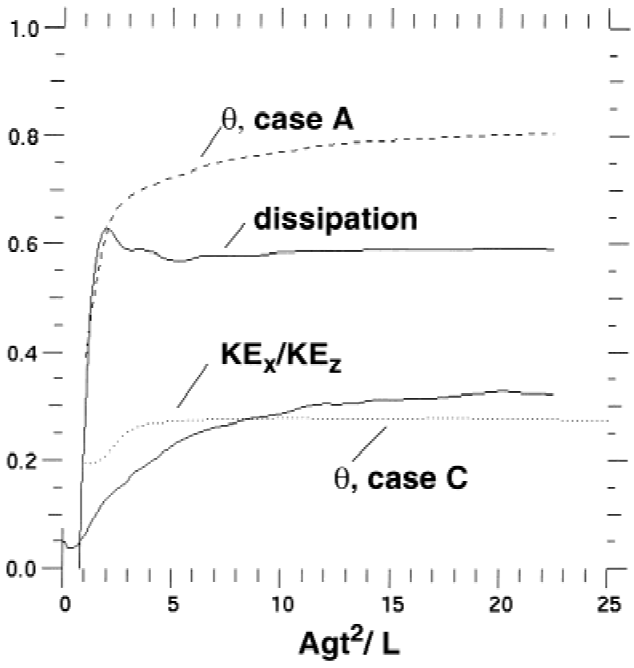

Fig. 7. Atomic mixing parameter, θ, versus Agt^2/L for case A (dashed), and for case C simulation with interface reconstruction (dotted). Also shown are the fraction of the potential energy drop that has been dissipated and the ratio of the kinetic energy in the x (spanwise) direction to that in the z (streamwise) direction, both for case A.

ACKNOWLEDGMENTS

This work was performed under the auspices of the U.S. Department of Energy by the University of California, Lawrence Livermore National Laboratory under contract No. W-7405-Eng-48.

REFERENCES

Annuchina, N.N. *et al.* (1978). Turbulent mixing at an accelerating interface between liquids of different densities. *Izv. Akad. Nauk. SSSR, Mekh Zhidk Gaza* **6**, 157–160.

Clark, T. & Harlow, F.H. (2002). Modeling radiation effects in mixing layers. *Proc. 8th International Workshop on the Physics of Compressible Turbulent Mixing*, (Schilling, O., Ed.). Livermore, CA: Lawrence Livermore National Laboratory.

Cook, A.W. & Dimotakis, P.E. (2001). Transition stages of Rayleigh–Taylor instability between miscible fluids. *J. Fluid Mech.* **443**, 69–99.

Dimonte, G. & Schneider, M. (2000). Density ratio dependence of Rayleigh–Taylor mixing for sustained and impulsive acceleration histories. *Phys. Fluids* **12**, 304–321.

Dimonte, G., Youngs, D.L., Dimits, A., Weber, S., Marinak, M., Wunsch, S., Garasi, C., Robinson, A., Andrews, M.J., Ramaprabhu, P., Calderl, A.C., Fryxell, B., Biello, J., Dursil, L., MacNeice, P., Olson, K., Ricker, P., Rosner, R., Timmes, F., Tufo, H., Young, Y.-N. & Zingale, Y.-N. (2003). A comparative study of the turbulent Rayleigh–Taylor (RT) instability using high-resolution 3D numerical simulations: The Alpha-Group collaboration. Submitted to *Phys. Fluids*.

Glimm, J., Grove, J.W., Li, X.L., Oh, W & Sharp, D.H. (2001). A critical analysis of Rayleigh–Taylor growth rates. *J. Comp. Phys.* **169**, 652–677.

Hecht, J., Offer, D., Alon, U., Shvarts, D., Orsag, S.A. &

https://doi.org/10.1017/S0263034603213264 Published online by Cambridge University Press

McCrory, R.L. (1995). Three-dimensional simulations and analysis of the nonlinear stage of the Rayleigh–Taylor instability. *Laser Part. Beams* **13**, 423–440.

Lindl, J. (1995). Development of the indirect-drive approach to inertial confinement fusion and the target physics basis for ignition and gain. *Phys. Plasmas* **2**, 3933–4024.

Marinak, M.M., Tipton, R.E., Landen, O.L., Murphy, T.J., Amendt, P., Haan, S.W., Hatchett, S.P., Keane, C.J., McEachern, R. & Wallace, R. (1996). Three-dimensional simulations of Nova high growth factor capsule implosion experiments. *Phys. Plasmas* **3**, 2070–2076.

Marinak, M.M., Kerbel, G.D., Gentile, N.A., Jones, O., Pollaine, S., Dittrich, T.R. & Haan, S.W. (2001). Three-dimensional HYDRA simulations of National Ignition Facility targets. *Phys. Plasmas* **8**, 2275–2280.

Rayleigh, J.W.S. (1900). *Scientific Papers*, Vol. II, p. 200. Cambridge, UK: Cambridge University Press.

Read, K.I. (1984). Experimental investigation of turbulent mixing by Rayleigh–Taylor instability. *Physica D* **12**, 45–58.

Taylor, G.I. (1950). The instability of liquid surfaces when accelerated in a direction perpendicular to their plane. *Proc. R. Soc. London, Ser. A* **201**, 192–196.

Young, Y.-N., Tufo, H., Dubey, A. & Rosner, R. (2001). On the miscible Rayleigh–Taylor instability: Two and three dimensions. *J. Fluid Mech.* **447**, 377–408.

Youngs, D.L. (1984). Numerical simulation or turbulent mixing by Rayleigh–Taylor instability. *Physica D* **12**, 32–44.

Youngs, D.L. (1994). Numerical simulation of mixing by Rayleigh–Taylor and Richmyer–Meshkov instabilities. *Laser Part. Beams* **12**, 725–750.

https://doi.org/10.1017/S0263034603213264 Published online by Cambridge University Press